ECS Transactions, 25 (8) 541-548 (2009)
10.1149/1.3207637 ©The Electrochemical Society

Deposition of WN_xC_y from the Tungsten Piperidylhydrazido Complex $Cl_4(CH_3CN)W(N\text{-pip})$ as a Single-Source Precursor

Dojun Kim,[a] Oh Hyun Kim,[a] Hiral M. Ajmera,[a] Tim Anderson,[a]
Jürgen Koller,[b] and Lisa McElwee-White[b]

[a] Department of Chemical Engineering, University of Florida, Gainesville, Florida 32611 USA
[b] Department of Chemistry, University of Florida, Gainesville, Florida 32611 USA

The tungsten piperidylhydrazido complex $Cl_4(CH_3CN)W(N\text{-pip})$ (**1**) was used as a single-source precursor for growth of tungsten carbonitride (WN_xC_y) by metal-organic chemical vapor deposition (CVD) in H_2 carrier. Multiple spectroscopic techniques were used for preliminary evaluation of the suitability of **1** as a precursor and to suggest possible fragmentation pathways. The effect of growth temperature on film microstructure, lattice parameter, average grain size, chemical composition, chemical bonding states, growth rate, film resistivity, and sheet resistance was studied.

Introduction

The present challenges in microelectronic integrated circuits are their speed and reliability. To meet these challenges as device dimensions continue to shrink, the industry is transitioning from Al to Cu interconnects in upper-level metallization to reduce RC time delays and improve reliability (1). Cu interconnects show greater resistance toward electromigration and 40 % lower resistivity, as compared to Al interconnects. This transition has required the development of barrier layers to prevent Cu transport since the presence of Cu in Si causes serious degradation of device performance associated with contact resistance, barrier height, *p-n* junctions, contact layers, and electrical connections (2). Cu also exhibits a high diffusivity in Si ($D_{Cu} \sim 2 \times 10^{-5}$ cm^2/s at 500 °C) and thus can affect large volumes of Si (3). Therefore, an effective Cu diffusion barrier is required to prevent Cu transport and intermixing in Si with adjacent dielectric materials for Cu interconnect technology. Ta/TaN bilayers deposited by physical vapor deposition (PVD) are currently utilized as Cu diffusion barriers in semiconductor device technology. Limitations of PVD due to the directional nature of deposition, however, produce conformality challenges as the barrier thickness decreases. WN_x films show good thermal stability with Cu, acceptably low resistivity when deposited by CVD, and reasonable behavior during chemical mechanical planarization (4). The ternary phase material, WN_xC_y, is also a promising candidate for diffusion barrier applications (5-7). This material exhibits lower electrical resistivity, good adhesion to Cu, very good resistance to Cu diffusion, and acceptable film growth on SiO_2. It is noted that it is not clear from the results of this study whether the W exists as a two-phase mixture of β-W_2N and β-WC_{1-x} or as the solid solution WN_xC_y. For consistency in this report, the W material is denoted as β-WN_xC_y.

Downloaded 26 Oct 2009 to 128.227.139.249. Redistribution subject to ECS license or copyright; see http://www.ecsdl.org/terms_use.jsp

Experimental Procedures

Precursor Synthesis

Precursor **1** was prepared as described in the literature (8).

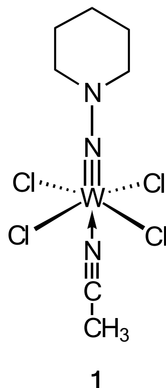

Figure 1. Structure of $Cl_4(CH_3CN)W(N\text{-pip})$ (**1**).

Film Growth

Due to the low volatility of the precursor **1**, aerosol-assisted CVD (AACVD) was used for film growth of this refractory metal nitride (9). The solid precursor **1** in benzonitrile solution (8.1 mg/mL) was filled into a syringe and pumped into a nebulizer. The nebulizer forms a precursor aerosol from the solution. A vertical, quartz cold-wall CVD reactor was used to deposit thin films on *p*-type, boron-doped Si(100) substrates with electrical resistivity of 1 - 2 Ω-cm. Precursor aerosol in H_2 carrier was delivered to the substrate placed on a graphite susceptor, which was heated by radio-frequency (rf) induction coils in the temperature range 300 to 700 °C. The operating pressure was maintained at 350 Torr. The H_2 (99.999%, Airgas) carrier gas flow rate was 1000 sccm and the deposition time was 150 min.

Film Characterization

XRD (Philips APD 3720) was used to identify the crystalline phase of the films and measure the structural properties. XPS (Perkin-Elmer PHI 5600 ESCA) was used to identify the chemical composition and bonding states of the elements in the film. Prior to XPS measurements, the as-grown samples were sputter cleaned for 10 min using Ar^+ ions to remove residual surface contaminants. An SEM (JEOL JSM-6335F) was used to view the film thickness and surface morphology. The sheet resistance of the film was measured by four-point probe (Alessi Industries).

Results and Discussion

Preliminary Precursor Screening

Multiple spectroscopic techniques were applied to evaluate the viability of **1** as a precursor for WN_xC_y deposition (8). Positive-ion chemical ionization (CI) mass spectrometry was performed to obtain some insight into the fragmentation behavior of **1**. The absence of molecular ion peaks is in good agreement with the acetonitrile ligand

Downloaded 26 Oct 2009 to 128.227.139.249. Redistribution subject to ECS license or copyright; see http://www.ecsdl.org/terms_use.jsp

being labile. Mass envelopes containing the piperdine moiety ($[pip]^+$ and $[H_2pip]^+$) were observed in high abundance, suggesting that cleavage between the two hydrazido N atoms is facile under high energy conditions (ionization during MS or pyrolysis during CVD). Studies of **1** via thermogravimetric analysis (TGA) showed a drop in mass corresponding to loss of the acetonitrile ligand at approximately 100 °C.

Film Microstructure

The XRD spectra [Fig. 2(a)] show the evolution of film crystallinity with increasing deposition temperature. The four observed reflections are well matched with a two-phase mixture of β-W_2N and β-WC_{1-x} phases or their solid solution β-WN_xC_y with the same face-centered-cubic (fcc) structure. The observation of film growth by X-SEM and the absence of XRD peaks attributable to β-WN_xC_y for films deposited from 300 to 450 °C, lead to the conclusion that amorphous material was deposited in this temperature range. The polycrystalline peaks appearing in spectra of material deposited from 500 to 700 °C indicate no preferred crystal orientation. Primary peaks at 37.24 and 42.98 2θ° are consistent with (111) and (200) orientation, while the other two peaks at 62.58 and 74.98 2θ° originate from the (220) and (311) reflections, respectively. As the deposition temperature increases to 700 °C, the (111) and (200) β-WN_xC_y peaks sharpen. The ability to deposit amorphous films of WN_xC_y at low temperature is important for diffusion barrier applications since the formation of polycrystalline films facilitates transport of Cu across the barrier to the underlying Si via the grain boundaries.

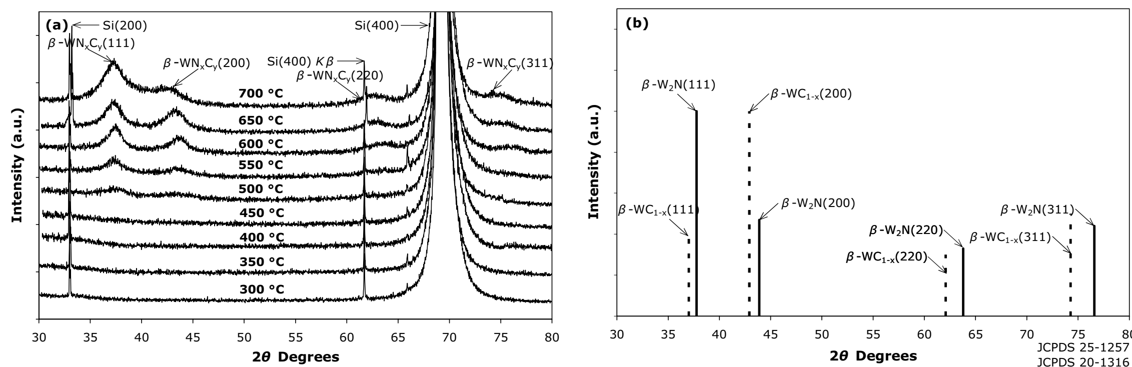

Figure 2. XRD spectra for films deposited from **1** on Si(100) in H_2 carrier: (a) between 300 and 700 °C, and (b) standard diffraction plots for β-W_2N and β-WC_{1-x}.

Chemical Composition

XPS results for chemical composition [Fig. 3(a)] show that W, N, C, and O were present in the films. No Cl contamination in the deposited material was observed within the detection limit of XPS (~ 1 at. %). The W level is highest for deposition temperature between 450 and 500 °C, while the N, C, and O levels are relatively constant in this range. From 300 to 400 °C, the C level is below 10 at. %, with the lowest level of 6 at. % for deposition at 400 °C. Between 500 and 700 °C, the C level increases gradually from 15 to 67 at. %. The overall trend for C content is consistent with more rapid decomposition of hydrocarbon groups in both the precursor and the solvent as the growth temperature increases, leading to increased C incorporation into the film. As the deposition temperature increased from 300 to 400 °C, the N level increased from 10 to 18 at. %, however, above 500 °C the N level decreases. Typically, refractory metal nitride

Downloaded 26 Oct 2009 to 128.227.139.249. Redistribution subject to ECS license or copyright; see http://www.ecsdl.org/terms_use.jsp

diffusion barriers show a decreasing tendency for N incorporation with increasing deposition temperature due to N_2 desorption (10). With the addition of C, there is also increased competition from C bonding at W adsorption sites. When the deposition temperature reaches 700 °C, the N level has declined to ~5 at. %. Films deposited at 300 °C show over 20 at. % O, which significantly decreases to 14 at. % at 450 °C. As the deposition temperature increased from 450 to 700 °C, the O level decreased gradually to 5 at. %. The polycrystalline microstructure shown in Fig. 2(a) becomes evident for depositions performed at 500 °C. As the deposition temperature increases, the average grain size increases as well. The microstructure becomes more crystalline, which inhibits post-growth incorporation of O into the lattice of the film (11). This result is attributed to the densification of film by grain growth between 500 to 700 °C.

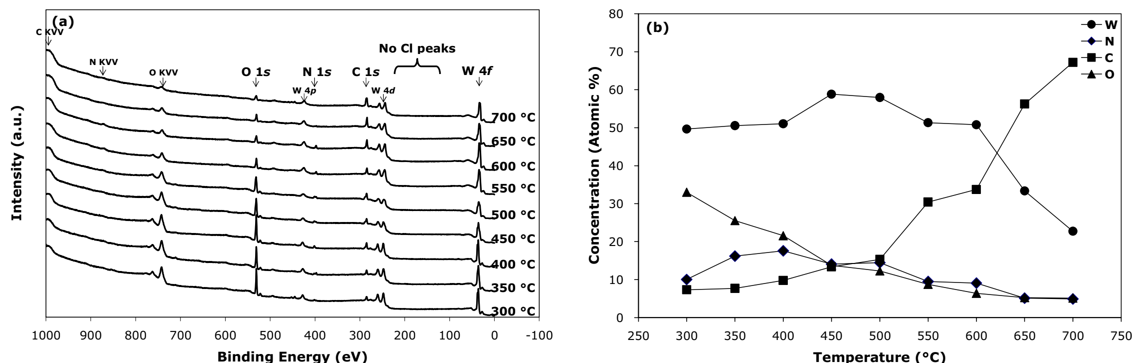

Figure 3. (a) XPS spectra for films deposited on Si(100); (b) Variation in chemical composition of W, N, C, and O content in the films with deposition temperature.

Chemical Bonding States

XPS was used to measure the binding energy (BE) of atoms in the films. The XPS spectra [Fig. 4(a)] reveal the evolution of the W 4*f* BE region as the deposition temperature changes. The major W $4f_{7/2}$ and W $4f_{5/2}$ peaks at 400 °C are at 31.6 and 33.5 eV, which are close to values for WC_x and WN_x (Table I). These two values are higher than those for metallic W and lower than those for WO_3. These BE values are between the reference peaks of WN_x and WC_x, indicating W is bonded to both C and N. As the deposition temperature rises to 700 °C, the BE increases to 31.8 and 33.8 eV, which correspond to WC_x and WN_x as well. For material deposited at 300 °C, the BE more closely resembles that of WO_3 but shifts toward values for WC_x or WN_x as the deposition temperature rises to 350 °C. This indicates a chemical bonding state shifting from WO_3 dominant to WN_xC_y as the deposition temperature increases from 300 to 700 °C. Figure 4(b) illustrates the change of the XPS spectra in the region of the N 1*s* BE as the deposition temperature changes. The N 1*s* peak is observed at 397.3 eV in each spectrum, which is in the range of reported values for WN_x (Table I). Hence, the N in the film is bound as WN_x. N at the grain boundary can be excluded as a second peak associated with it (~399 eV) is not observed within the detection limit of XPS. The maximum N intensity is seen in the spectra of films deposited at 400 °C, which is consistent with the high N level in those films.

Figure 4(c) reveals the evolution of the XPS spectra in the region of the C 1*s* BE for several values of deposition temperature. The trend with increasing deposition temperature is increasing intensity and higher BE of the C 1*s* peaks. Between 300 and 600 °C, the BE is lower than the reported value for amorphous C, while above 600 °C,

Downloaded 26 Oct 2009 to 128.227.139.249. Redistribution subject to ECS license or copyright; see http://www.ecsdl.org/terms_use.jsp

the BE is higher than that of WC_x. Deconvolution of the broad C 1*s* peak at 700 °C yields two separate peaks, which are at 283.1 and at 284.5 eV. The peaks at the lower BE are attributed to C in β-WN_xC_y bonding states, while the peaks at higher BE are consistent with the presence of amorphous C. For deposition at temperature higher than 650 °C, a small amount of amorphous C is evident along with WC_x and WN_x in the film. As the deposition temperature increases to 700 °C, an increasing amount of amorphous C co-exists with WC_x in the film.

Figure 4(d) displays the dependence of the XPS spectra in the region of the O 1*s* BE as a function of the deposition temperature. A single O peak was observed near 530.5 eV in each spectrum, which is consistent with the presence of WO_3 (Table I). O levels are higher in films grown at low temperature due to diminished film crystallinity and C incorporation. As the deposition temperature increases to 700 °C, the film density is increased by crystallization and the grain boundaries are infiltrated by C incorporation.

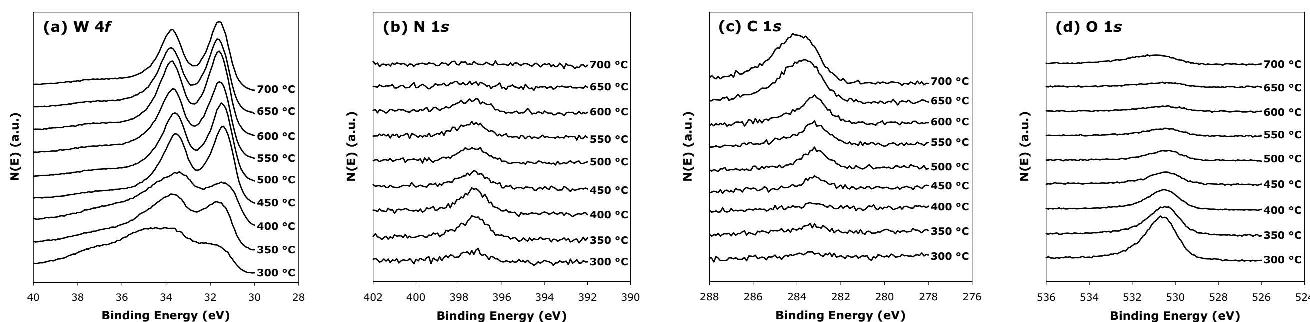

Figure 4. Change of binding energies in (a) W 4*f*, (b) N 1*s*, (c) C 1*s*, and (d) O 1*s* with deposition temperature.

Table I. Reported binding energy (BE) values

Compound	W $4f_{7/2}$	W $4f_{5/2}$	N 1*s*	C 1*s*	O 1*s*	References
WN_x	32.7–33.6	33.3-35.8	396.2-398.2			(12-16)
WC_x	31.6-32.3	33.7-33.9		279.7-283.8		(15-18)
WO_3	35.5-36.7	37.6-37.8			528.2-531.6	(12, 15, 16, 19, 20)
Metallic W	31.2-31.7	33.4				(15-17)
N at grain boundary			399.2-400.0			(19, 21)
Amorphous C				284.2-285.2		(15, 16, 22)

Lattice Parameter and Average Grain Size

The lattice parameter was determined by XRD using the 2θ position of the β-WN_xC_y(111) diffraction peaks. The lattice parameter [Fig. 5(a)] shows an increasing tendency as deposition temperature increases from 500 to 650 °C. This change is consistent with C incorporation in the polycrystalline solid solution β-WN_xC_y, and not at the grain boundaries. The C level continues to increase with deposition temperature above 500 °C [Fig. 3(b)]. Between 650 and 700 °C, however, the lattice parameter decreases. In this range, the C level increases while W decreases with almost no compositional change in N and O [Fig. 3(b)]. The decrease in lattice parameter between 650 and 700 °C is consistent with C incorporation at the solubility limit in β-WN_xC_y and this limit decreasing with increasing temperature (23). This conclusion is supported by the chemical bonding states [Fig. 4(c)], where the C 1*s* peak in this range is shifted to higher BE and has a broad peak that can be deconvoluted into two separate peaks attributed to the formation of amorphous C in addition to the β-WN_xC_y phase.

The average grain size was calculated using Scherrer's equation (24). The most dominant β-WN_xC_y(111) diffraction peak of the four characteristic polycrystalline peaks

Downloaded 26 Oct 2009 to 128.227.139.249. Redistribution subject to ECS license or copyright; see http://www.ecsdl.org/terms_use.jsp

was used to determine FWHM as the reference peak in the calculation. The average grain size [Fig. 5(b)] increases between 500 and 600 °C, varying from 31 to 47 Å.

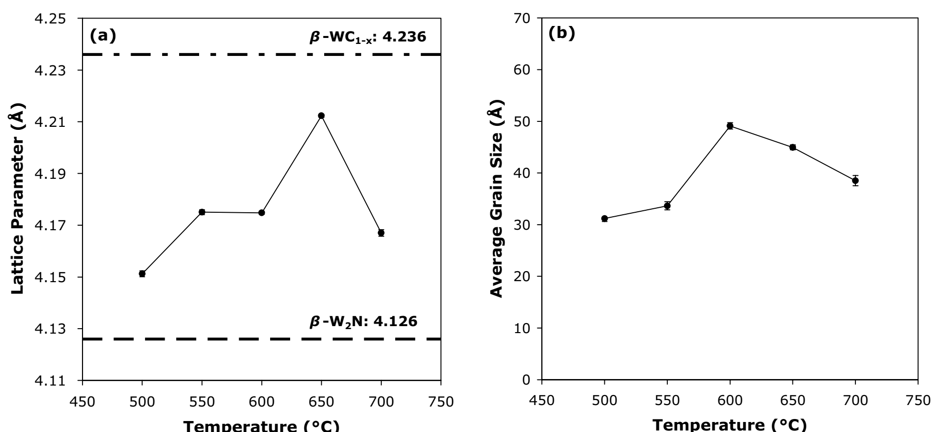

Figure 5. Change in (a) lattice parameter and (b) average grain size with deposition temperature for polycrystalline films based on β-WN_xC_y(111) diffraction peaks.

Growth Rate

The growth rate is in the range of 2.7 to 29.4 Å/min, as determined by cross-sectional SEM. For films deposited between 650 and 700 °C, the growth rate significantly increased suggesting a change in the growth mechanism at these temperatures. This observation was supported by the detection of amorphous C over 600 °C. In addition to this high temperature growth region, the plot (Fig. 6) shows the presence of two growth regimes. The region with the shallow slope between 450 °C and 600 °C is typical of a mass transfer limited growth regime. The region with the steep slope is a kinetically controlled growth regime between 300 °C and 450 °C.

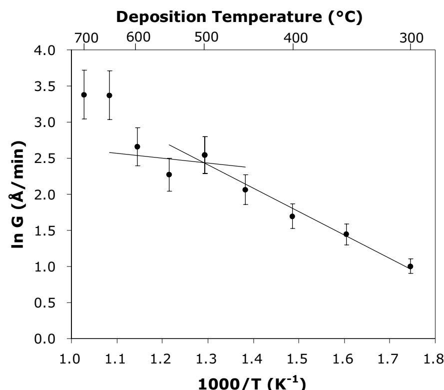

Figure 6. Change in growth rate with deposition temperature.

Electrical Resistivity and Sheet Resistance

Figure 7(a) shows the variation of film resistivity with deposition temperature. The lowest resistivity is 0.9 mΩ-cm at 550 °C and the value of film resistivity fluctuates with the interplay of grain growth, C content, O content, and film thickness between 500 and 700 °C. As shown in Fig. 3(b), an increase in the amorphous C level as the deposition temperature increases from 650 to 700 °C results in an increase in electron scattering, which causes the film resistivity to increase. The highest film resistivity is 9.4 mΩ-cm

Downloaded 26 Oct 2009 to 128.227.139.249. Redistribution subject to ECS license or copyright; see http://www.ecsdl.org/terms_use.jsp

for films deposited at 350 °C. The high N level in those films is consistent with increased film resistivity in the β-WN_xC_y polycrystalline structures, which is due to the higher resistivity for β-W_2N relative to β-WC_{1-x}.

Film resistivities obtained depend on both the sheet resistance and thickness of the films. The sheet resistance was plotted with deposition temperature to decouple the influence of film thickness on electrical properties [Fig. 7(b)]. The sheet resistance increases sharply with deposition temperature from 370 Ω/□ at 300 °C to 1480 Ω/□ at 350 °C. This increase is consistent with oxide formation. As deposition temperature increases to 550 °C, the sheet resistance decreases to 60 Ω/□ due to lower O and higher C content. The value of the sheet resistance fluctuates with increasing deposition temperature above 550 °C, but eventually become stable near 70 Ω/□ at 700 °C.

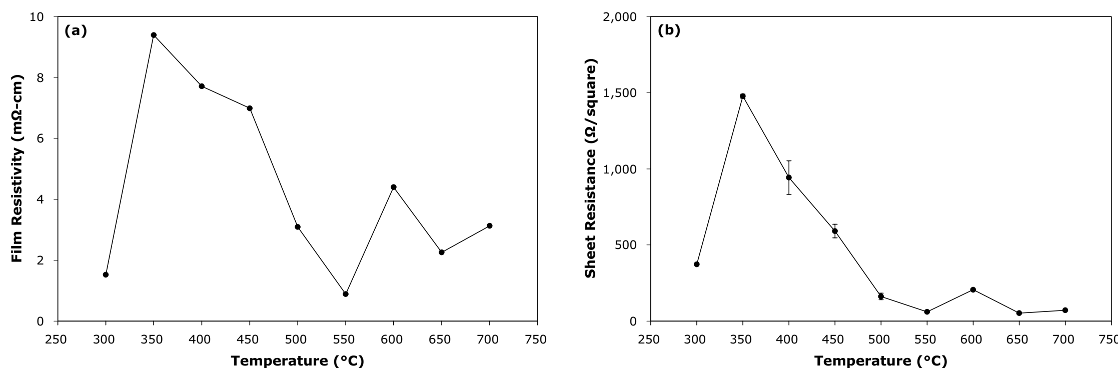

Figure 7. Change in film resistivity and sheet resistance with deposition temperature.

Conclusions

The tungsten piperidylhydrazido complex $Cl_4(CH_3CN)W(N\text{-}pip)$ (**1**) was used as a single-source precursor for film growth of WN_xC_y to investigate film properties relevant to diffusion barrier applications. XRD results suggest that films deposited at temperature below 500 °C are X-ray amorphous and films deposited at higher temperature are polycrystalline. The XPS data on the W 4*f* bonding state are consistent with W present in WN_xC_y and WO_3. For films deposited at the low end of the temperature range, WO_3 predominates and as the deposition temperature increases, WN_xC_y becomes the dominant W species. XRD results, however, do not indicate any WO_3 peaks. The XPS data on the N 1*s* bonding state suggest that N is present in WN_x. while results on the C 1*s* bonding state indicate that C is present in WC_x and as amorphous C. For depositions at temperature higher than 650 °C, amorphous C co-exists with WC_x. The XPS data on the O 1*s* bonding state suggests that O is present in WO_3 and the O levels are the highest for growth temperature below 400 °C. As the deposition temperature varies, the film growth rate increases from 2.7 to 29.4 Å/min, with the transition from a kinetically controlled growth regime to a mass transfer controlled regime occurring near 550 °C. Film resistivity changes with the interplay of grain growth, C and O content, and film thickness. Further diffusion barrier testing and film characterization are in progress.

Acknowledgments

We would like to thank the National Science Foundation for support under NSF-CRC Grant CHE-0304810. We also would like to thank the Major Analytical Instrumentation Center (MAIC) at the University of Florida for assistance with XPS, XRD, and SEM.

Downloaded 26 Oct 2009 to 128.227.139.249. Redistribution subject to ECS license or copyright; see http://www.ecsdl.org/terms_use.jsp

References

1. E. Kolawa, P. J. Pokela, J. S. Reid, J. S. Chen and M. A. Nicolet, *Appl. Surf. Sci.*, **53**, 373 (1991).
2. M. Wittmer, *Appl. Phys. Lett.*, **36** (6), 456 (1980).
3. A. A. Istratov, *J. Electrochem. Soc.*, **149(1)**, G21 (2000).
4. N. Gonohe, *Mater. Trans.*, **43** (7), 1585 (2002).
5. K.-E. Elers, V. Saanila, W.-M. Li, M. Soininen, J. T. Kostamo, S. Haukka, J. Juhanoja and W. Besling, *Thin Solid Films*, **434** (1-2), 94 (2003).
6. S. Smith, W.-M. Li, K.-E. Elers and K. Pfeifer, *Microelectron. Eng.*, **64** (1), 247 (2002).
7. A. M. Hoyas, J. Schuhmacher, C. M. Whelan, T. F. Landaluce, D. Vanhaeren and K. Maex, *J. Appl. Phys.*, **100** (11) 114093-1 (2006).
8. J. Koller, H. M. Ajmera, K. A. Abboud, T. J. Anderson and L. McElwee-White, *Inorg. Chem.*, **47**, 4457 (2008).
9. L. McElwee-White, *Dalton Trans.*, (45), 5327-5333 (2006).
10. H. P. Kattelus, E. Kolawa, K. Affolter and M. A. Nicolet, *J. Vac. Sci. Technol. A*, **3** (6), 2246 (1985).
11. P. J. Pokela, C. K. Kwok, E. Kolawa, S. Raud and M. A. Nicolet, *Appl. Surf. Sci.*, **53**, 364 (1991).
12. H. L. Zhang, D. Z. Wang and N. K. Huang, *Surf. Coat. Technol.*, **115** (2-3), 140 (1999).
13. Y. G. Shen and Y. W. Mai, *Mat. Sci. Eng. B-Solid*, **76** (2), 107 (2000).
14. J. S. Lee, C. S. Park, J. Y. Kang, D. S. Ma and J. Y. Lee, *J. Vac. Sci. Technol. B*, **8** (5), 1117 (1990).
15. C. D. Wagner, W. M. Riggs, L. E. Davis, J. F. Moulder and G. E. Muilenberg, *Handbook of X-ray Photoelectron Spectroscopy*, Perkin-Elmer Corporation, Eden Prairie, MN (1978).
16. J. F. Moulder, W. F. Stickle, P. E. Sobol and K. D. Bomben, *Handbook of X-ray Photoelectron Spectroscopy*, Physical Electronics, Eden Prairie, MN (2000).
17. R. J. Colton and J. W. Rabalais, *Inorg. Chem.*, **15** (1), 236 (1976).
18. G. Leclercq, M. Kamal, J. M. Giraudon, P. Devassine, L. Feigenbaum, L. Leclercq, A. Frennet, J. M. Bastin, A. Lofberg, S. Decker and M. Dufour, *J. Catal.*, **158**, 142 (1996).
19. T. Nakajima, K. Watanabe and N. Watanabe, *J. Electrochem. Soc.*, **134** (12), 3175 (1987).
20. P. J. C. Chappell, M. H. Kibel and B. G. Baker, *J. Catal.*, **110**, 139 (1988).
21. M. Nagai and K. Kishida, *Appl. Surf. Sci.*, **70-1**, 759 (1993).
22. V. Crist, *Handbook of Monochromatic XPS Spectra: The Elements and Native Oxides*, John Wiley & Sons, New York, NY (2000).
23. O. J. Bchir, S. W. Johnston, A. C. Cuadra, T. J. Anderson, C. G. Ortiz, B. C. Brooks, D. H. Powell and L. McElwee-White, *J. Cryst. Growth*, **249**, 262 (2003).
24. B. D. Cullity and S. R. Stock, *Elements of X-ray diffraction*, 3rd ed., Prentice Hall, Upper Saddle River, NJ (2001).

Downloaded 26 Oct 2009 to 128.227.139.249. Redistribution subject to ECS license or copyright; see http://www.ecsdl.org/terms_use.jsp